

Optical Engineering

OpticalEngineering.SPIEDigitalLibrary.org

Simulations of multiwavelength cladding pumping of high-power fiber Raman amplifiers

Nan Zhao
Soonki Hong
Achar V. Harish
Yutong Feng
Johan Nilsson

SPIE.

Nan Zhao, Soonki Hong, Achar V. Harish, Yutong Feng, Johan Nilsson, "Simulations of multiwavelength cladding pumping of high-power fiber Raman amplifiers," *Opt. Eng.* **58**(10), 102701 (2019), doi: 10.1117/1.OE.58.10.102701.

Simulations of multiwavelength cladding pumping of high-power fiber Raman amplifiers

Nan Zhao,^{a,b} Soonki Hong,^{a,*} Achar V. Harish,^a Yutong Feng,^a and Johan Nilsson^a

^aUniversity of Southampton, Optoelectronics Research Centre, Southampton, United Kingdom

^bSouth China Normal University, Current address Guangzhou Key Laboratory for Special Fiber Photonic Devices, Guangzhou, China

Abstract. We numerically simulate and optimize a high-power fiber Raman amplifier cladding pumped by spectrally combined diode lasers at wavelengths from ~ 0.9 to $\sim 1 \mu\text{m}$ in the continuous-wave regime. This amplified a signal at the first-Stokes wavelength of 1024 nm. We found that it was possible to add pumps over an increasingly wide wavelength span up to ~ 90 nm, while still maintaining an incremental conversion efficiency higher than 60%, even though the Raman linewidth is only ~ 15 nm. We investigated the dependence on the power of individual diode lasers and on the wavelength spacing and found that the total conversion efficiency reaches $\sim 70\%$ with realistic pump sources based on state-of-the-art diode lasers. We believe this study shows the potential for high-power fiber Raman lasers pumped by spectrally combined multiwavelength diode and fiber laser sources. © The Authors. Published by SPIE under a Creative Commons Attribution 4.0 Unported License. Distribution or reproduction of this work in whole or in part requires full attribution of the original publication, including its DOI. [DOI: [10.1117/1.OE.58.10.102701](https://doi.org/10.1117/1.OE.58.10.102701)]

Keywords: fiber Raman amplifier; high power fiber laser; nonlinear optics; wavelength combining.

Paper 190388SS received Mar. 19, 2019; accepted for publication Jun. 25, 2019; published online Sep. 25, 2019; corrected Aug. 18, 2020.

1 Introduction

Stimulated Raman scattering (SRS) can be an efficient process for generation and amplification of light in optical fibers. For power scaling, pumping with multimode laser diodes has recently been demonstrated in multimode as well as double-clad (DC) fibers.^{1,2} This approach combines the well-established and well-controlled fabrication, the potentially high resilience to photodarkening, and the high damage threshold of “passive” high-silica fibers (e.g., germanosilicate fibers) with the simplicity of high-power, direct-diode laser pumping, the brightness enhancement enabled by DC fibers, and the advantages of SRS such as wavelength-agility, immunity to high-energy self-Q-switching, and nonlocal gain saturation.³ However, SRS is a relatively weak process, so high diode brightness and pump intensity are required to reach sufficient Raman gain. This can be analyzed in terms of a figure of merit (FoM), given by the induced peak Raman gain relative to the background loss, i.e., $I_P g_R(\nu_{\text{peak}})/\alpha$, where I_P is the pump intensity, $g_R(\nu)$ is the Raman gain coefficient, ν_{peak} is the frequency shift to the Raman gain peak, and α is the fiber background loss, which for simplicity is sometimes assumed to be the same for pump and signal. It was found that a value of the FoM of at least five¹ was needed for efficient conversion in an ideal cavity, whereas a higher value would be required in laser cavities and amplifiers with excess loss or high gain. Today’s continuous-wave (cw) diode lasers can provide 140 to 200 W of output power at 0.9 to 1 μm from a 105- μm core pigtail at an NA of 0.15. In combination with a low-loss fiber with a low-Ge-concentration core (e.g., NA < 0.1) and a pure-silica inner-cladding with NA of 0.3 and thus inner-cladding diameter of 52.5 μm to accommodate the pump, this allows for an FoM of around 10, which is adequate for efficient conversion. There is however an additional requirement for efficient conversion in cladding-pumped fiber Raman

sources (including amplifiers). The inner-cladding/core area ratio must not exceed approximately eight, insofar as cascaded SRS to higher Raman orders is to be avoided.⁴ An inner cladding diameter of 52.5 μm thus requires a core diameter of at least 18.6 μm . Larger cores and thus inner claddings are possible, but make it increasingly difficult to maintain single-mode operation. Thus, the standard power-scaling approach of an increasing number of pump ports on a pump combiner with an increasingly large common port to reach targeted power is limited by the limited brightness of diode-laser pump sources and the limited core size for single-mode operation. We note also that a pump combiner degrades the pump brightness.⁵ This may render the brightness inadequate even with state-of-the-art multimode diode lasers. An alternative route to further power-scaling is then to use a brighter pump source, e.g., a Yb-doped fiber laser, which excels in this regard.⁶ Another potential route to high-brightness pumping is to spectrally combine diode lasers at different wavelengths. Such diode laser sources are pursued vigorously for direct-diode materials processing.^{7–9} This makes spectrally combined diode lasers attractive candidates for cladding-pumping of fiber Raman sources, which retains the attractions of pumping directly with diode lasers.

However, the pump acceptance bandwidth of SRS in high-silica fibers is limited to the Raman linewidth of ~ 5 THz (~ 15 nm at 1 μm) in the conventional case of the first-order Raman conversion with high Raman gain coefficient g_R , i.e., when the pump wavelength is separated from the Stokes wavelength by approximately the peak Raman shift ν_{peak} . This is around 12 to 15 THz in silica, corresponding to 400 to 500 cm^{-1} or ~ 40 to 50 nm at 1 μm . Pumping with any single wavelength within the pump acceptance bandwidth is expected to allow for efficient operation of a high-silica fiber Raman device. Likewise, pumping with spectrally combined pump lasers with a wavelength span below 15 nm is expected to behave similarly as single-wavelength pumping, with similar efficiency. However, the 15-nm

*Address all correspondence to Soonki Hong, E-mail: s.hong@soton.ac.uk

pump acceptance bandwidth for (effectively) single-wavelength pumping is much smaller than the wavelength range of spectrally combined diode laser sources for materials processing. This is largely determined by the wavelength range over which diode lasers perform best and may be 50 to 100 nm. Interestingly, however, high-efficiency pumping over a wavelength range exceeding the 15-nm Raman linewidth has been demonstrated recently, through pumping on several Raman orders¹⁰ as well as through dual-wavelength pumping with 26-nm wavelength separation. This separation is significantly larger than the Raman linewidth but still different from the peak Raman shift.¹¹ Though the 26-nm span is still inadequate for many spectrally combined diode lasers, these results still suggest there may be considerable potential for pumping at multiple wavelengths over spans exceeding the Raman peak shift, even at off-resonance wavelengths which are not necessarily carefully selected and do not correspond to the Raman peak shift, or multiples thereof.

In this paper, we present simulation results of multiwavelength cladding-pumping in the 0.9- 1- μm wavelength range of a high-power fiber Raman amplifier (FRA) in the continuous-wave regime, with fixed and optimized pump wavelength spacings of 5 to 30 nm. We use a signal in the first Stokes order of the longest-wavelength pump and reach up to 71% conversion efficiency with narrow optimized pump wavelength spacing at a single-pump FoM of 10 (200 W per pump wavelength). The efficiency remains above 68% for up to 10 pump wavelengths. Furthermore, for all considered FoMs (between 10 and 80), the efficiency can be higher with two pump wavelengths, and often with more than two, than with only one pump wavelength. Depending on the value of the FoM, the efficiency can remain higher than the efficiency with a single pump laser up to a span of 100 nm. Our work thus confirms the potential for multiwavelength diode-laser off-resonance pumping with total pump bandwidth significantly larger than the Raman linewidth for further power scaling and improved efficiency of diode-laser-pumped fiber Raman sources. Notably, this applies to important multi-kW spectrally combined diode-laser sources in rapid development for direct-diode materials processing.

2 Theory and Simulation Model

Figure 1 shows the layout of the multiwavelength-pumped FRA we simulate. A signal seed and a multiwavelength pump are combined and launched, respectively, into the core and inner cladding of a DC FRA in the same (forward) direction. All pump and Stokes waves are unpolarized. The first,

longest-wavelength, pump is always at 980 nm, with additional pumps added at predetermined or optimized wavelengths on the short side of 980 nm. The signal is seeded by 10 W at around 1024 nm, which corresponds to the Raman gain peak (i.e., first Stokes order) with 980-nm pumping. The DC Raman fiber has a 19.1- μm -diameter core with low Ge-doping in a 54- μm -diameter, pure silica inner cladding, for an area ratio of eight. A larger area ratio allows for higher-power pumping, but in the absence of spectral filtering, this leads to cascaded Raman conversion into higher Stokes orders, which in the case of single-wavelength pumping significantly reduces the conversion efficiency into the first Stokes for area ratios larger than eight.⁴ Thus, although we include such cascaded conversion to the second and third Stokes orders in our simulations, it is a parasitic process relative to amplification of a signal in the first Stokes order. All reported efficiencies relate to the first-Stokes signal power. The Raman gain spectrum and fiber loss spectrum we used are adopted from Refs. 12 and 13 and are shown in Fig. 2, for silica fiber with low Ge-content. To account for pump wavelength and polarization, we scaled $g_R(\nu)$ with the inverse of the pump wavelength,¹² and reduced it by half for unpolarized pumping. The pump power is the same for each wavelength, and can be 200, 400, 800, and 1600 W per wavelength, corresponding to FoM of 10, 20, 40, and 80. Here, and throughout this paper, we calculate the FoM based on the power of a single pump wavelength, 980 nm, where the propagation loss becomes 1.92 dB/km and the Raman gain coefficient 51 fm/W. The diode lasers at other wavelengths are assumed to have the same power but different loss and Raman gain coefficients according to Fig. 2. Furthermore, even for a fixed Raman frequency shift, the Raman gain coefficient is approximately inversely proportional to pump wavelength.¹² Therefore, the FoMs at other pump wavelengths differ somewhat from that at 980 nm. Whereas current state-of-the-art diode lasers are bright enough for 200 W single-wavelength pump power and FoM = 10, higher power may be difficult to achieve at present. However, spectrally combined Yb-doped fiber lasers would be able to reach FoM = 80, for pumping in the 1- to 1.1- μm wavelength range.

With multiwavelength pumping, SRS between pumps, between pumps and Stokes, and between different Stokes orders need to be taken into consideration. Equation (1) describes the evolution of the pump and Stokes powers for a discrete number n of interacting waves in the continuous-wave (time-independent) regime

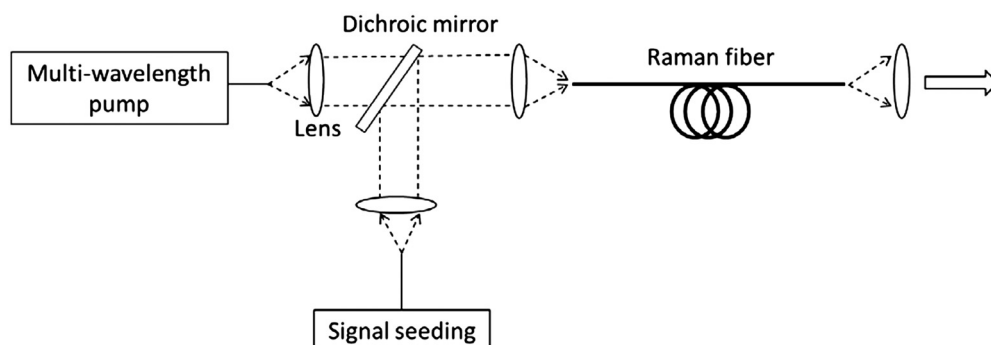


Fig. 1 Layout of simulated multiwavelength-pumped FRA.

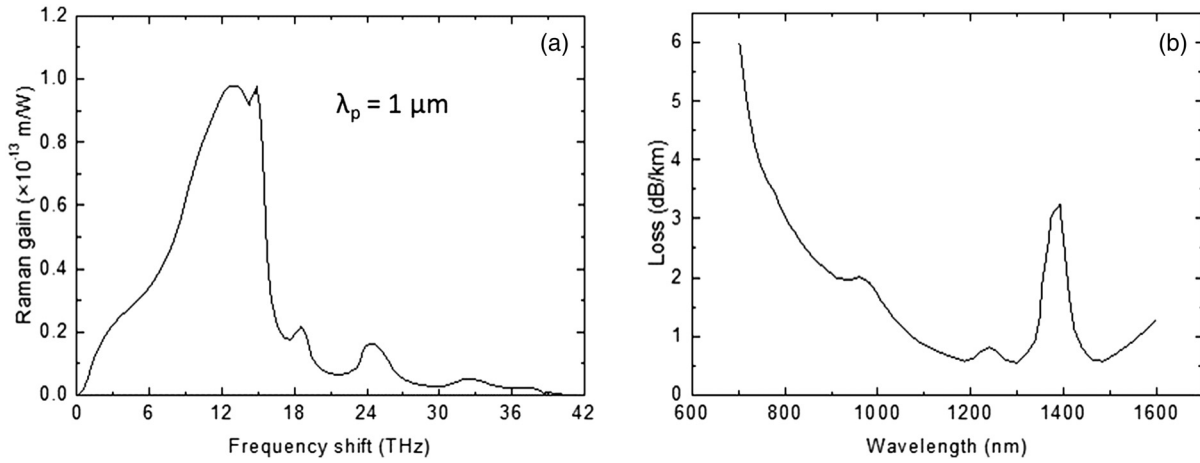


Fig. 2 (a) Spectral dependence of Raman gain coefficient $g_R(\nu)$ versus Raman frequency shift ν for silica fiber with polarized pumping at wavelength $\lambda_p = 1 \mu\text{m}$.¹² (b) Silica fiber loss spectrum.¹³

$$\frac{dP_i}{dz} = -\alpha_i P_i + \sum_j G_{ij} P_i P_j. \quad (1)$$

Here, i and j vary from 1 to n , P_1 to P_{n-3} are pump powers, P_{n-2} to P_n are Stokes powers in the first, second, and third Stokes order (relative to the longest-wavelength pump at 980 nm), and α_i represents the fiber loss. Furthermore, if ν_k is the optical frequency of wave k and $g_{ij} = g_R(|\nu_i - \nu_j|)$:

$$\begin{cases} G_{ij} = +g_{ij}/A_{\text{eff}} & \text{if } \nu_i < \nu_j \text{ (gain for signal } i) \\ G_{ij} = 0 & \text{if } \nu_i = \nu_j \\ G_{ij} = -(g_{ij}/A_{\text{eff}})(\nu_i/\nu_j) & \text{if } \nu_i > \nu_j \text{ (depletion of pump } i) \end{cases} \quad (2)$$

$$\begin{cases} A_{\text{eff}} = A_{\text{core}} & \text{if } i \text{ and } j \text{ are both in core} \\ A_{\text{eff}} = A_{\text{clad}} & \text{if } i \text{ or } j \text{ is in cladding.} \end{cases} \quad (3)$$

We implemented Eqs. (1)–(3) in Matlab using a Runge-Kutta solver (Matlab ODE45) for numerical integration. The Matlab code is short and straightforward to write. We then used it to evaluate multiwavelength-pumped FRAs with different parameters. In all cases, we chose the fiber length to yield the highest conversion into the first Stokes. Note that there is no backward-propagating light due to unseeded SRS or Rayleigh scattering in our model, and therefore no coupling between counterpropagating waves. Therefore, the solution of Eq. (1) as integrated in the forward direction is at every position equal to the output power distribution of a fiber of the corresponding length. The computer run-times for determining the optimum length and the corresponding output power for a given set of input wavelengths and powers are therefore small, typically less than 1 s on a standard personal computer.

Our simulations do not treat individual spatial modes, but rather assume that the pump powers are distributed uniformly over the whole core and cladding area. Although each pump mode has a different overlap with the core, a practical, well-designed cladding-pumped fiber should counteract mode-selective pump depletion through mode-coupling and/or noncircular cladding geometries. Although the relatively small inner cladding leads to large mode spacings that

hamper mode-coupling, mode-coupling is still expected to be significant, given the fiber lengths needed for SRS. An interesting question is what effect cascaded Raman conversion of the pump has on the spatial pump homogeneity, but this is beyond the scope of this paper.

As it comes to the core, this could in principle be strictly single-mode, for strictly single-mode signal propagation. However, this requires a core-NA of 0.041 or less, for which the waveguiding may be too weak. Therefore, we assume an NA of 0.1. The core then supports around eight modes, but it may still allow for fundamental-mode operation, if higher-order signal modes are not excited at the launch and mode-coupling is small (due to the relatively large mode-spacing in a 19.1- μm core). Although the effective area of the signal depends somewhat on the partition of power between modes, we neglect this and use the core area as the effective area for cascaded SRS from the first Stokes order to higher orders. These are seeded by vacuum fluctuations of power 14.8 μW for the second Stokes wave at 1073 nm and 14.1 μW for the third Stokes wave at 1126 nm. These levels correspond to the power in eight modes in two polarizations within a gain bandwidth of 5 THz. Bendloss-filtering¹⁴ could perhaps suppress higher-order modes in the Stokes orders; this has not been considered.

3 Results

Figure 3 shows the power evolution of the waves along a fiber simulated with our model for an FoM of 10 with 10 pumps separated by 10 nm. The evolution as well as the conversion efficiency depends on the parameters, but this is a representative example. In the beginning of the fiber, SRS transfers power from the pumps at shorter wavelengths to those at longer wavelengths, and most of all to the longest-wavelength one at 980 nm. The first-Stokes signal grows from the start, and at some point, reaches a power where it depletes the 980-nm pump so fast that also the 980-nm pump power decreases. The first Stokes also amplifies the second Stokes (seeded by vacuum fluctuations). Once the first-Stokes wave has reached sufficient power, the second-Stokes wave grows rapidly, and rapidly depletes the first Stokes. Then, the SRS cascades to the third Stokes and would continue to higher orders, but those are not included in our simulations. The power and the length at the first-Stokes

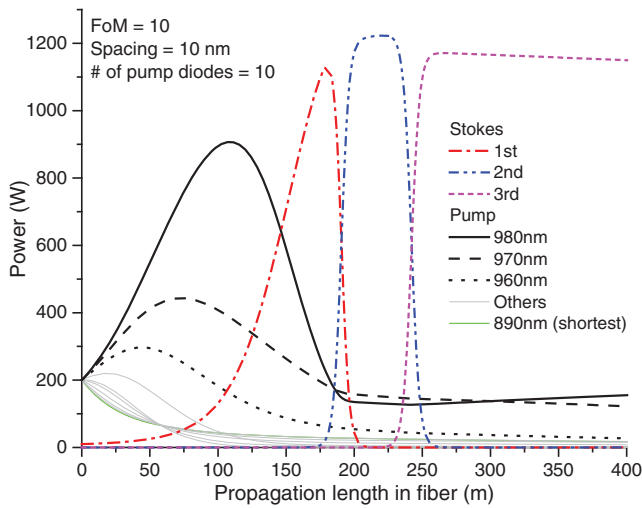


Fig. 3 Power evolution of waves vs. propagation length in fiber for the case of FoM = 10 with 10 nm-spaced 10 diodes. Because all waves propagate in one direction, the powers for a given propagation length are equal to the output powers for a fiber of that length.

peak were taken as the signal output power and optimized length throughout this paper. Note that the maximum power of second Stokes is 5% to 10% higher than that of first Stokes due to a considerable amount of residual pump. During the depletion of the first-Stokes power, SRS continues to transfer power from the pumps to the first-order Stokes, and this

power will add to the second-Stokes power, which thus can reach a higher level than that of the first Stokes.

Incomplete pump depletion occurs also for single-wavelength cladding-pumping, when the area ratio exceeds around eight, because the smaller effective area and thus higher rate of SRS from the first to second Stokes than from the pump to the first Stokes. Multiwavelength pumping reduces the overall rate of SRS from the pumps to the first Stokes and thus exacerbates this problem. For the area ratio of eight used here, the residual pump power when the first-order Stokes power reaches its maximum varies from 17% to 66% of the total power, depending mainly on the wavelength spacing but also on the FoM. If we only consider cases with conversion efficiency above 60%, then the leakage varies in the range 17% to 30%. It is possible to counteract this with a smaller area ratio. For an area ratio of four, the residual pump power range reduces to 6% to 55% (6% to 18% for cases that reach over 60% conversion efficiency), and the maximum powers of the first and second Stokes become almost the same.

Figure 4 shows the first-Stokes conversion efficiency obtained with 5, 10, 15, 20, and 30 nm pump wavelength spacing, for different FoMs and number of pumps. The first-Stokes signal was seeded at a fixed wavelength of 1024 nm, i.e., 438 cm^{-1} or 13.1 THz from the longest pump-wavelength. Throughout this paper, each pump laser is either on or off. Thus, the pump power increases in discrete steps, and the lines between data points only serve to guide the eye. As expected, a narrower spacing generally allows for

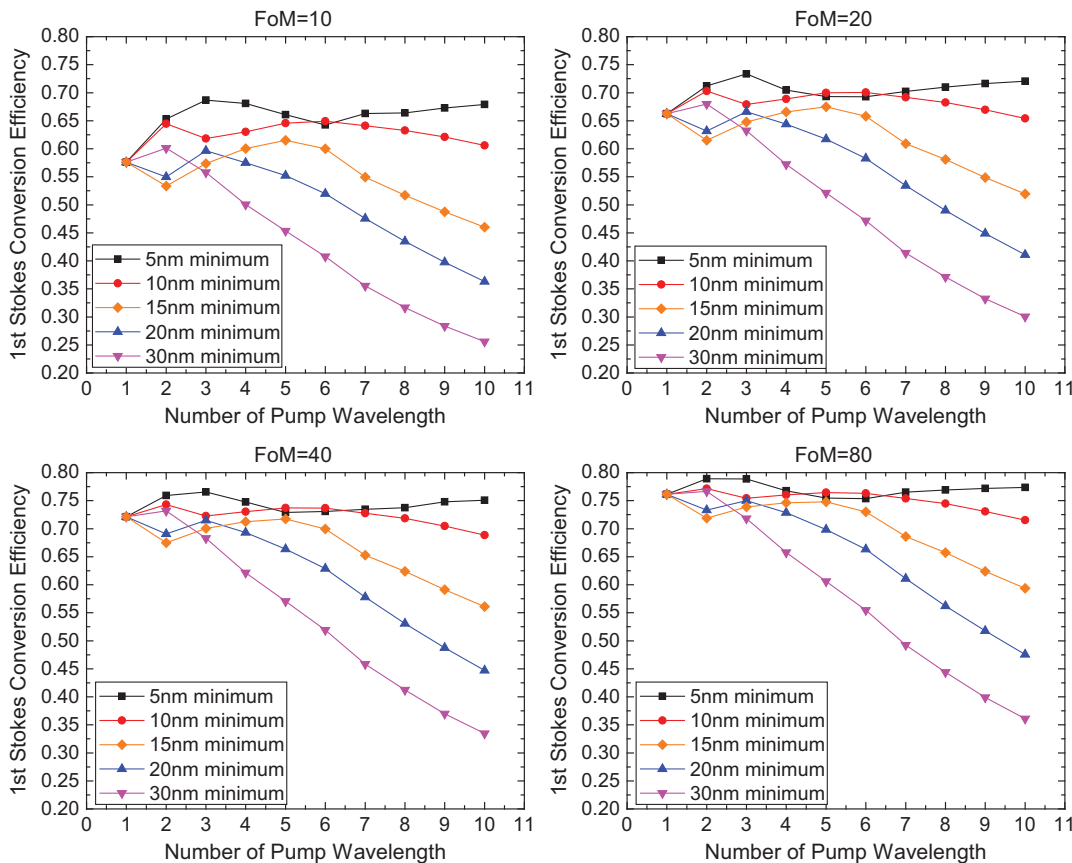


Fig. 4 Conversion efficiency to first-Stokes with 5, 10, 15, 20, and 30 nm pump wavelength spacing at different pump powers as represented by different FoM.

higher conversion efficiency. Furthermore, in many cases, multiwavelength-pumping allows for higher conversion efficiency than single-wavelength pumping does, especially for small FoMs and narrow wavelength spacing. The efficiency remains high with 5 and 10 nm spacings even with 10 pump sources, which is the highest number we considered. The total pump bandwidth of up to 90 nm (31 THz) is then considerably larger than the conventional pump acceptance bandwidth of ~ 5 THz, and even exceeds twice the shift to the Raman gain peak. The 31-THz bandwidth is approximately equal to the maximum Raman frequency shift in Fig. 2(a), but we believe this is a coincidence. The efficiency stays largely above 55%, 65%, 70%, and 72% for FoM of 10, 20, 40, and 80, respectively. For 5-nm spacing, for those FoMs, the efficiency stays above 65%, 70%, 73%, and 75%, respectively, for 2 to 10 pumps. By contrast, for 20 to 30 nm spacings, the efficiency deteriorates rapidly as the number of pumps increases. Note also that whereas InGaAs diode lasers are available with largely constant specifications from ~ 0.9 to $\sim 1 \mu\text{m}$, the largest total wavelength range in Fig. 2 is 270 nm. This range is difficult or impossible to cover with diode lasers of adequate performance.

Whereas the trends in Fig. 4 for the dependence on the number of pump wavelengths, wavelength spacing, and FoM are expected, some details are less clear and suggest that further improvements are possible. For 15- and 20-nm spacings, two wavelengths are worse than one and three. Furthermore, 30 nm is significantly better than 20-nm spacing for two pumps, and there are also other examples where

a larger wavelength spacing is comparable to, or better than, a smaller spacing. A smaller spacing is more difficult to achieve, so a larger spacing is more attractive in those cases (subject to diode laser availability).

To investigate if such anomalies can be avoided, and if further improvements are possible, we next consider the case of optimized pump wavelengths. This is shown in Fig. 5, for different numbers of pump diodes, and with different minimum wavelength-spacings of 5, 10, 15, 20, and 30 nm. This requires nonlinear optimization. We used the Matlab routine FMINCON to optimize the wavelength spacings under the constraint of a minimum spacing and with the longest pump wavelength fixed at 980 nm. Also, the signal wavelength was optimized over a wavelength span corresponding to the first-Stokes peak. Thus, the number of optimization variables is equal to the number of pump wavelengths. In the optimization procedure, for a given set of wavelength spacings and signal wavelength, the signal output power in the first Stokes is calculated as in the fixed-wavelength case, and the maximum signal power, at the optimum length for this set of spacings and signal wavelength, is returned to the optimization procedure. This is repeated until the optimization procedure has found a set of wavelength-spacings and signal wavelength that maximizes the signal power. This will be a local maximum, since nonlinear optimization is not guaranteed to find the global maximum, but the results can be sanity-checked through the character of plotted curves. Furthermore, FMINCON was several times with different starting spacings and signal wavelengths. In all cases, the

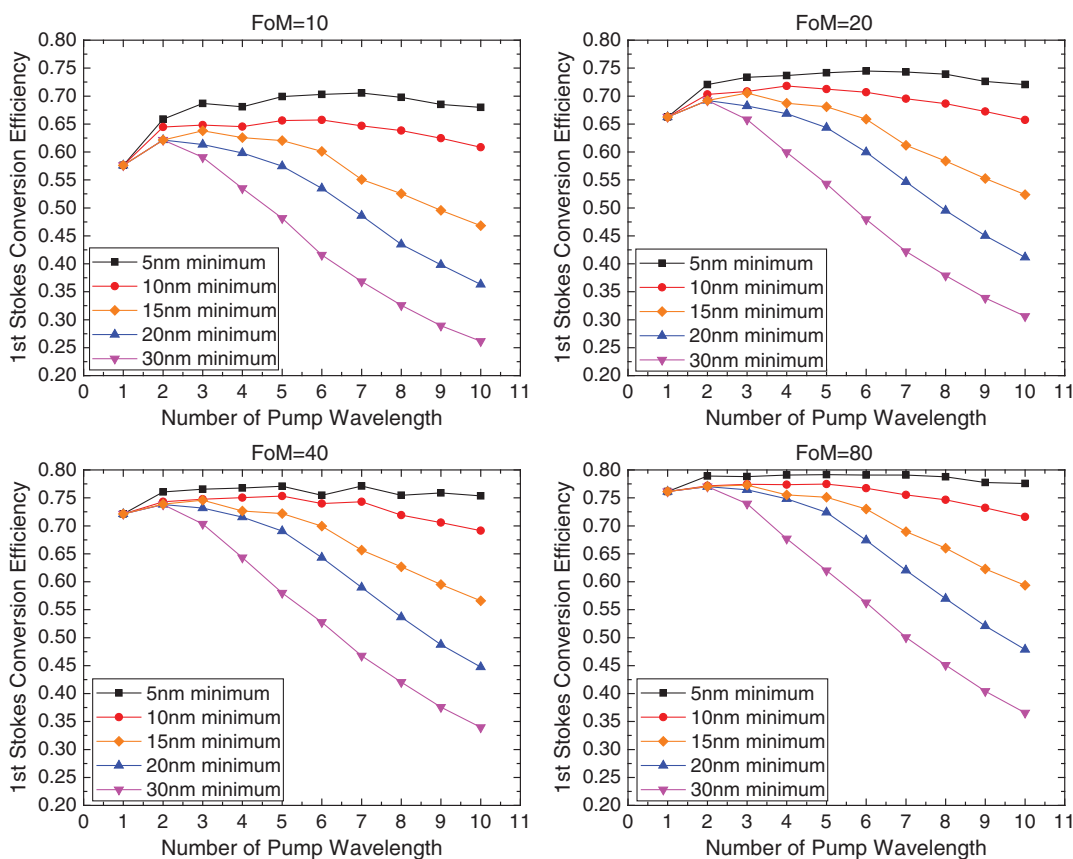


Fig. 5 Optimized first-Stokes conversion powers with 5-, 10-, 15-, 20-, and 30-nm minimum pump wavelength spacings at different pump powers.

minimum spacing was included as one starting set, so this set will always be included in the optimization procedure. Figure 5 shows that a smaller minimum spacing is better, but the minimum value would be dictated by the capabilities of the spectral combination technology. Furthermore, the anomalies are gone, except perhaps for some minor dips in efficiency in some cases. These and other minor anomalies in our results may be caused by imperfect optimization.

In all cases, two pump wavelengths are better than a single pump wavelength. Furthermore, with 5-nm minimum spacing, multiwavelength pumping is for all considered FoMs and number of diodes more efficient than single-wavelength pumping. Up to 68% efficiency is maintained with FoM = 10 even with the number of pumps extending to 10. The quantum conversion efficiency becomes 73%.

The first-Stokes output power dependence on the total pump power is plotted in Fig. 6, as we increase the number of pumps, both for nonoptimized fixed and optimized minimum pump wavelength spacings. This is based on the same data as used for Figs. 4 and 5, with equal pump power at each wavelength, but recalculated in terms of total pump power and first-Stokes output power. Since the different FoMs correspond to different amounts of pump power in each wavelength, the increment between data points is different for the different FoMs. The general conclusion is that there is little difference between fixed and optimized wavelength spacings, although there are a few cases in which the difference is nonnegligible. For the 5- to 10-nm cases, optimized as well as fixed, the output power increases almost linearly when adding more pump power by adding more wavelengths.

No roll-off is observed even for 10 pumps. The slope efficiency is $\sim 70\%$, 73% , 76% , and 78% for FoM = 10, 20, 40, and 80 with 5-nm minimum spacing. For 10 nm, it is $\sim 62\%$, 66% , 69% , and 71% . Note that for example, an FoM of 10 with 5-nm spacing is more efficient than an FoM of 20 with 10-nm spacing. A possible explanation is that a smaller wavelength spacing with the same spectral power density allows for more routes for cascaded SRS, of which the most efficient ones are favored. For spacings of 15 to 30 nm, the output power rolls over to the point where there is no further increase for additional pump wavelengths. The higher loss at the shorter wavelengths used with large numbers of pumps contributes to this roll-over, and we note that the higher FoMs, which are less affected by loss, show slightly weaker roll-off. Note also that the highest signal power density in Fig. 6 exceeds $40 \text{ W}/\mu\text{m}^2$ and may well lead to optical damage. A larger signal core would reduce the signal power density.

The optimized fiber lengths corresponding to Fig. 5 are plotted in Fig. 7, for the case of optimized wavelength spacings. This confirms the significantly shorter fibers with higher FoM, as well as with increasing number of pumps. This is particularly beneficial for small FoM when the total background loss is large and explains at least in part why the case of FoM = 10 shows the biggest efficiency-improvement with dual-wavelength pumping in Fig. 5.

Compared to the 5-nm results without optimization in Fig. 4, the efficiency with optimization in Fig. 5 is increased by nearly 5%, for five and six pump wavelengths. By contrast, the improvement is less significant or even negligible

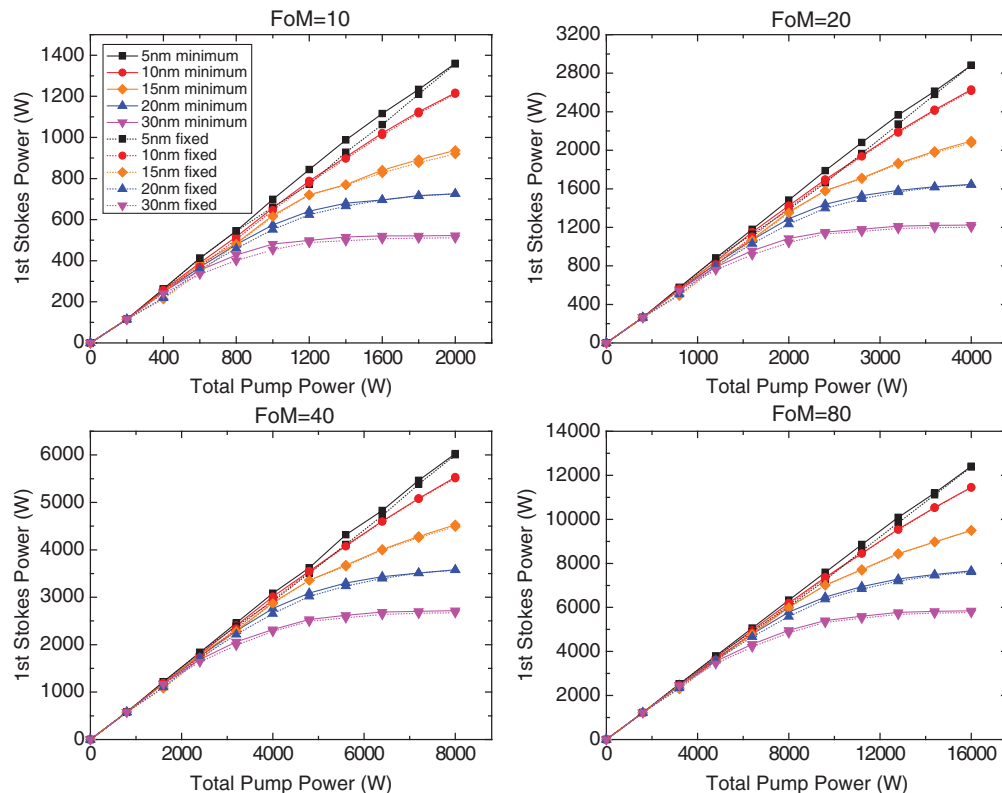


Fig. 6 First-Stokes output power versus total pump power with nonoptimized fixed and optimized minimum pump wavelength spacings of 5, 10, 15, 20, and 30 nm at different pump powers. Different FoMs correspond to different power per pump wavelength. The curves for fixed wavelengths are largely indistinguishable from those with optimized wavelengths.

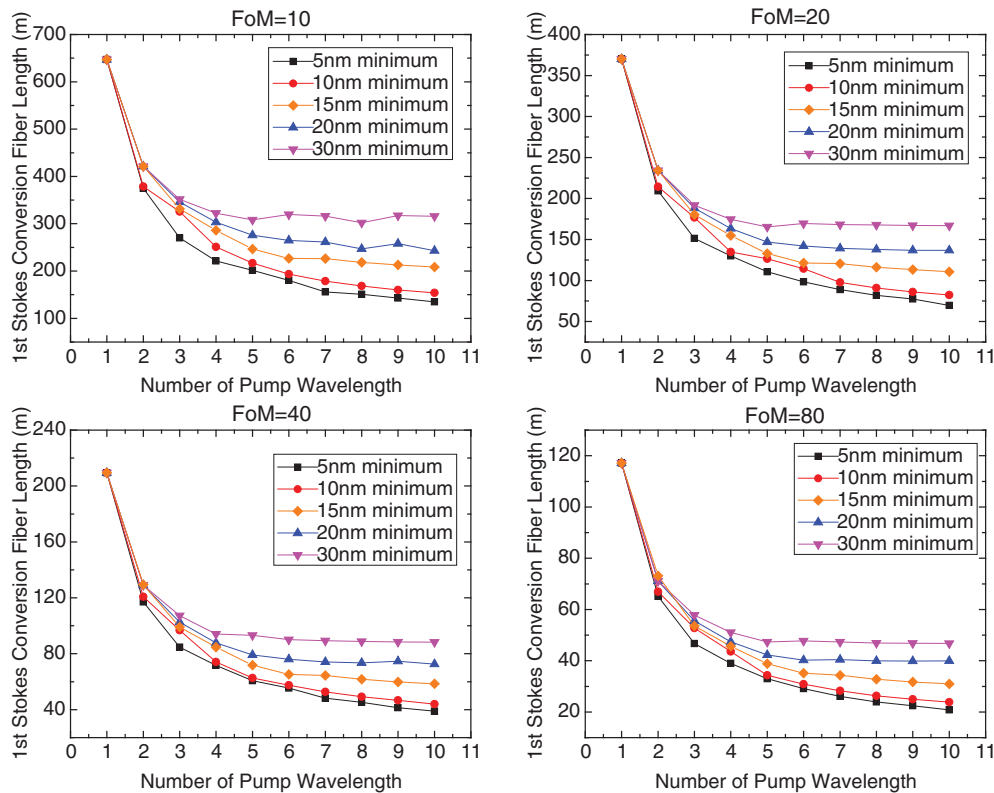


Fig. 7 Optimized first-Stokes conversion fiber length with 5-, 10-, 15-, 20-, and 30-nm minimum pump wavelength spacings at different pump powers.

for smaller as well as larger numbers of pump wavelengths, as well as for 15 to 30 nm spacing. This is also shown in Fig. 6. This is primarily a result of low efficiency in the case of five and six fixed wavelengths, so cannot be attributed to imperfect optimization. To help us understand why the optimization leads to bigger improvements for some combinations than for others, Fig. 8 plots the optimized wavelengths used in Fig. 5 for FoM = 10. For small pump numbers, the optimized wavelengths vary and, in some cases, lead to spacings approximately equal to the Raman peak shift, even when the minimum spacing is much smaller. When adding more pumps, the wavelength spacings are optimized to the minimum value, or close thereto, and thus close to the fixed spacing used in Fig. 4. For example, the pump wavelengths are optimized to 980, 954, and 934 nm for three pump sources with 20-nm minimum spacing. When pumped with 10 wavelengths, the spacings are at or close to the 20-nm minimum spacing. Other FoMs showed this pattern, too.

We conclude from Fig. 8 that for large numbers of pump wavelengths, the spacing should be as small as possible. Still, even with optimized spacings, Fig. 6 shows that the number of pumps that can contribute effectively is limited, at least in the case of large minimum spacings. This is also shown in Fig. 9, which plots the incremental conversion efficiency, defined as the increase in laser output power as a pump laser is added, relative to the power of that pump laser, for optimized spacings (fixed spacings gave similar results). In this case, the abscissa is the total wavelength span rather than the number of diodes. We note that in some cases in Fig. 8, the total pump wavelength range is smaller for a larger number of pumps. This affects the behavior of the curves in

Fig. 9. Furthermore, the differentiation used for Fig. 9 can exacerbate any unusual behavior in the optimization, or indeed in the physics of cascaded SRS. Nevertheless, overall, the decrease in incremental conversion efficiency for larger wavelength spans is similar for the different FoMs and minimum wavelength spacings. If we define the endpoint of the maximum usable wavelength span for pumping as the wavelength for which the output power increases by 60% of the power added by one diode then this becomes ~55, 76, 85, and 91 nm for FoM of 10, 20, 40, and 80, respectively. The span, $\Delta\lambda_{60}$, is plotted in Fig. 10 for 10, 20, and 30 nm minimum wavelength spacings. Surprisingly, the largest span is in most cases obtained for a 20-nm minimum spacing. Anomalous optimization is one of many effects that may explain this. One can also speculate that in some cases, the optimization or the nature of cascaded SRS means that the efficiency of the last diode within the bandwidth $\Delta\lambda_{60}$ may have a relatively weak dependence on the wavelength and may therefore shift significantly due to irregularities in the SRS cascade or the optimization. The incremental efficiency of an added diode laser also depends on the efficiency of the previous diode lasers. If this is below par then one can expect that the incremental efficiency an additional diode laser is higher than it would otherwise be, and possibly above rather than below the threshold of 60% used in Fig. 10. Thus, we believe the details of the curves are less significant than the bigger trends.

Figure 11 summarizes our results in terms of the relation between spectral power density, actual used bandwidth, and efficiency, for the case of optimized wavelength spacings. Points connected by lines correspond to similarly connected

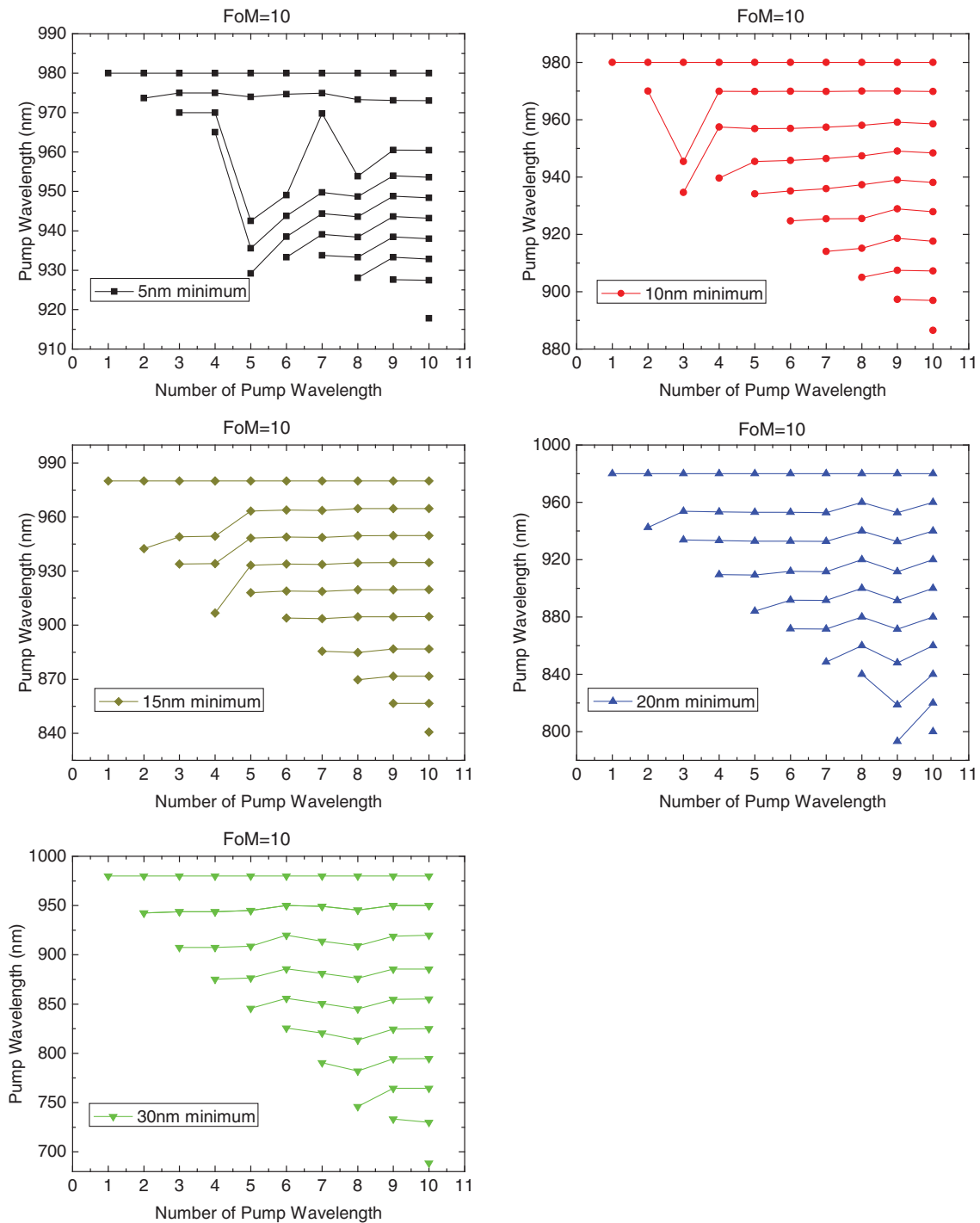


Fig. 8 Optimized pump wavelengths with 5-, 10-, 15-, 20-, and 30-nm minimum spacings at FoM = 10.

data points in Fig. 5. Only data points with bandwidths smaller than $\Delta\lambda_{60}$ are included. The spectral power density in Fig. 11 was calculated as $P_{tot}/[\Delta\lambda_R^2 + (\lambda_{max} - \lambda_{min})^2]^{1/2}$ where P_{tot} is the total pump power and λ_{max} ($=980$ nm) and λ_{min} are the wavelengths of longest and shortest pump wavelength. The expression also includes the intrinsic linewidth of SRS, $\Delta\lambda_R = 15$ nm. This prevents the spectral power density from diverging and ensures that it is the same regardless of the minimum pump spacing, in case of a single pump wavelength. The choice of $\Delta\lambda_R$ is motivated by the expected low dependence on the spectral distribution within a span of

$\Delta\lambda_R$, as a result of the fundamental properties of SRS. Nevertheless, the bandwidth in Fig. 11 is defined as $\lambda_{max} - \lambda_{min}$ (as in Figs. 9 and 10), i.e., the actual used bandwidth, since this relates to the combination technology rather than to the properties of SRS. For a given bandwidth, a higher spectral power density generally improves the efficiency. A higher spectral power density generally increases the bandwidth, as well, although in all cases, the efficiency drops at the largest bandwidths for a given FoM.

In Fig. 11, two wavelengths (from two diode lasers) are better than one, and the improvement can remain with a

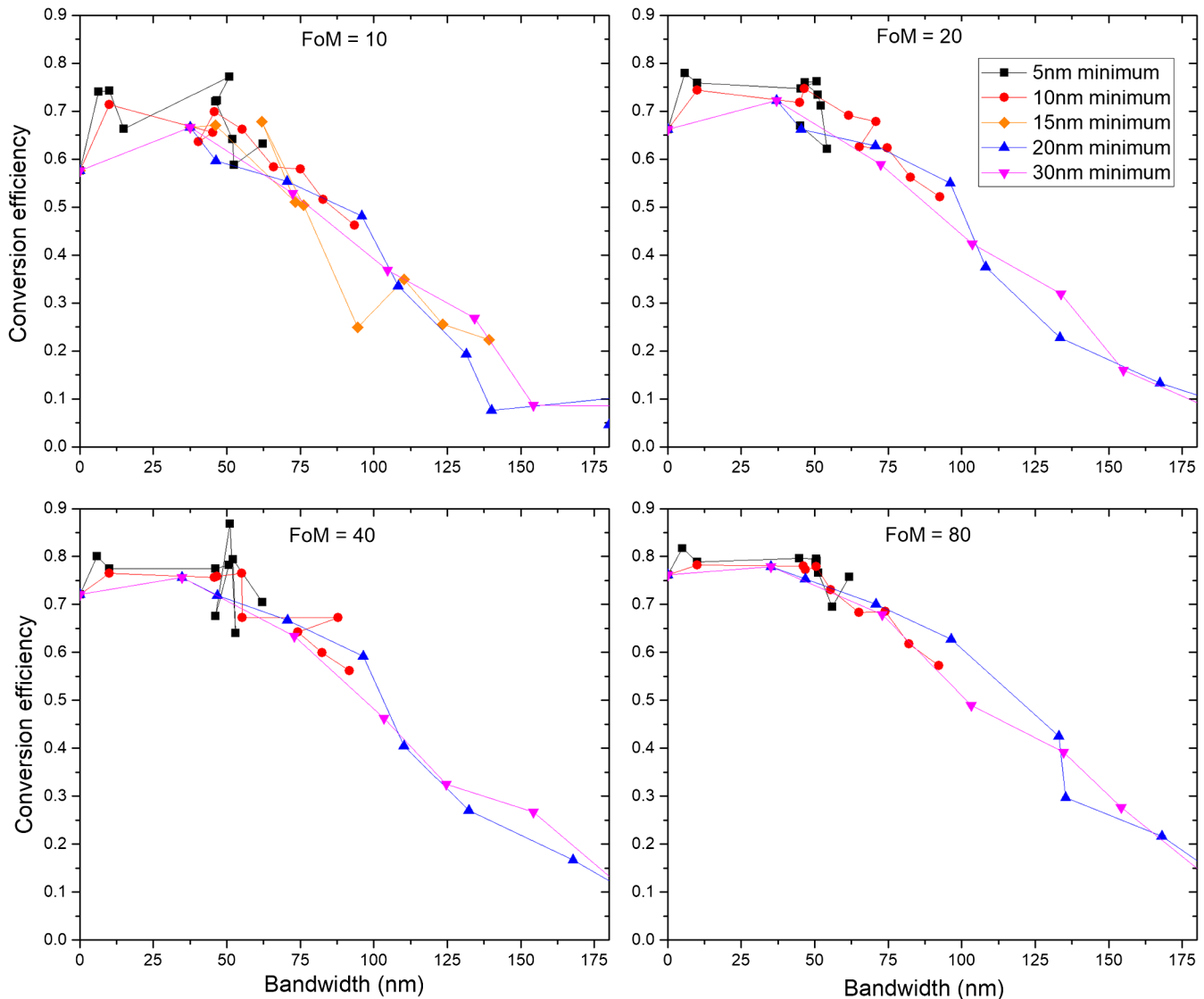


Fig. 9 Incremental conversion efficiency as pump lasers are added versus total pump bandwidth for FoM = 10, 20, 40, and 80.

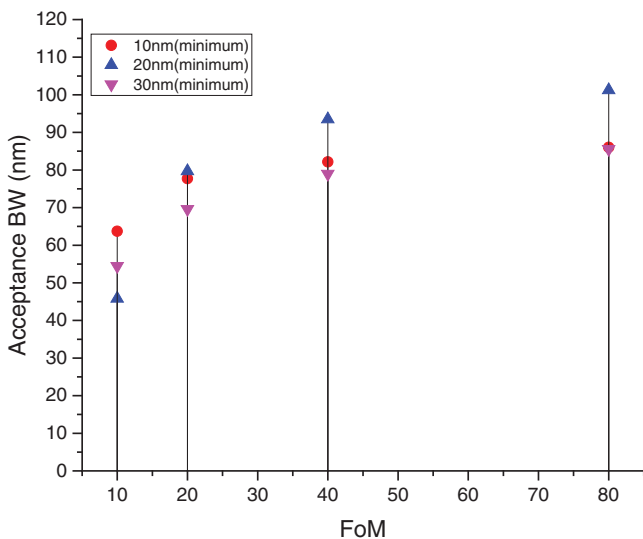


Fig. 10 Pump acceptance bandwidth $\Delta\lambda_{60}$ defined as the bandwidth for which the incremental conversion efficiency exceeds 60%, versus FoM for optimized pump wavelengths with different minimum spacings.

larger number of wavelengths, too. However, the improvement becomes smaller for larger FoM. It is easy to realize that for sufficiently high FoM, single-wavelength pumping will be more efficient than multiwavelength pumping. The Raman conversion losses stem from fiber background loss, quantum defect loss, and pump leakage. For high enough FoM (for high brightness or for low fiber loss), the quantum defect losses and/or the pump leakage will dominate, and in this regime, it is better to use narrow-band pumping close to the signal. Although we fall short of this regime even for an FoM of 80, which is very optimistic with diode-laser pumping, it may well be possible to reach it through pumping with a fiber laser, due to its exceptional brightness. Note however that it is difficult to maintain a high pump brightness through a fused-fiber pump combiner of the type often used for pumping of rare-earth-doped fibers.

It is also interesting to consider the effect of the Ge-concentration. Higher Ge-doping than assumed in this paper increases the Raman gain coefficient, but also the loss. The increase in the loss depends on wavelength, and we expect that at least for some wavelengths, the FoM can

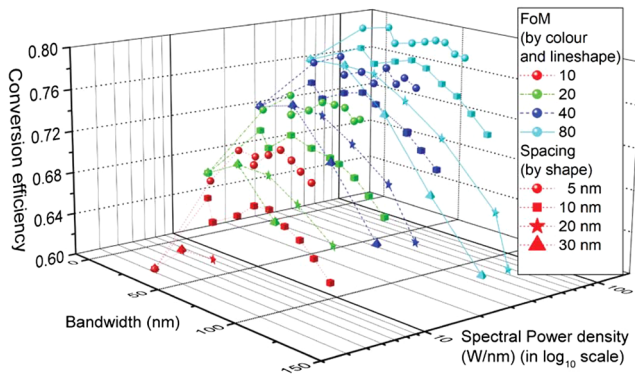


Fig. 11 Efficiency versus bandwidth and spectral power density for optimized wavelength spacings.

be higher with higher Ge-doping. However, the Raman linewidth and peak shift become smaller, which will also affect the efficiency of multiwavelength pumping. Further studies are needed to determine the effect of the Ge-concentration on multiwavelength pumping with different parameters.

As it comes to the spectral characteristics of the signal, our simulations assume that all power resides at either the pump wavelengths, the signal in the first-Stokes wavelength, or at the second or third Stokes orders. The spectrum of an individual wave, including the signal, is therefore not resolved. Spectral distortions of individual waves could occur through SRS as well as other nonlinearities¹² such as four-wave mixing (FWM) and self-phase modulation (SPM).^{15,16} However, simulations of SRS on a finer grid (not shown here) did not exhibit any SRS-induced line broadening. Although FWM was not included in the simulations, this requires phase-matching and is generally weak for multimode beams (the inner cladding supports ~ 700 modes LP-modes, i.e., around 1400 polarized modes). Even if the Stokes power resides in the fundamental mode, this has normal dispersion, which precludes phase-matched FWM between wavelengths in the same spatial mode. FWM to higher-order modes can still be possible, but with reduced strength because of the reduced overlap. SPM can still lead to significant broadening. In Fig. 3, at the output (i.e., where the first-Stokes signal peaks), the Raman gain of the second Stokes is ~ 60 dB. It follows that the nonlinear phase shift of the first-Stokes signal becomes $\gamma A_{\text{eff}}/g_R$ ($60/4.343$) rad = 35 rad, where γ is the nonlinear parameter that governs SPM. (This assumes all transfer of power to the second Stokes is from the first Stokes). Such large nonlinear phase shift can lead to significant spectral broadening. It is possible to reduce the resulting spectral broadening through improved amplitude stability; however, any multimode interference degrades the stability. Thus, it may be difficult to avoid spectral broadening of the signal in the fiber we consider. We note that a reduced area ratio reduces the SPM of the first Stokes, since this either reduces the signal intensity (in case of a larger core area) or the effective length (in case of a smaller inner-cladding area, which increases the pump depletion rate). Experimentally, in case of a GRIN fiber Raman laser which was core-pumped at 950 and 974 nm,¹¹ the first-Stokes emission linewidth was narrower than the intrinsic Raman linewidth even in the absence of any spectral filter.

This suggests conventional gain-narrowing managed to counteract line-broadening in this case.

We note that in addition to reducing the SPM of the first Stokes, a smaller area ratio also reduces the second-Stokes gain. Otherwise, the ~ 60 dB it reaches in our case may be enough to induce lasing from spurious reflections or possibly even double Rayleigh backscattering.^{17–19} We note also that temporal fluctuations of the first Stokes can also enhance the rate of conversion to the second Stokes.²⁰ Any increase in the rate of buildup of the second Stokes reduces the conversion efficiency into the first Stokes.

Our approach disregards the possibility that power is scattered to a wavelength outside the predefined wavelength set, although we observed this experimentally in Ref. 11. However, that was in a laser cavity, in which a relatively low Raman gain can lead to significant SRS. By contrast, insofar as the input power outside the predefined wavelengths is low (if the input spectrum is sufficiently pure), we expect that the Raman gain will be too low to lead to any significant power outside the predefined wavelengths, or in the backward direction.

We have not investigated the details of how a pump photon is converted to the first-Stokes signal. Figure 2(a) shows that direct conversion is possible for frequency differences of up to ~ 38 THz (from around 910 to 1024 nm), but with very low Raman gain coefficient. Therefore, except for the longest pump wavelengths, we expect that cascaded SRS dominates the conversion of pump photons to signal photons. When this happens, it is possible that the effective area becomes smaller in the cascade through so-called Raman beam cleanup.^{21–25} Our simulations do not include this effect. The details depend on the fiber design, but at least in principle, it opens up for larger area ratios for cascaded pumps.

4 Conclusion

We have used numerical simulations to investigate multiwavelength cladding-pumping directly with diode lasers of high-power FRAs operating on the first Stokes wavelength of the longest-wavelength pump. We find that compared to single pump laser, spectrally combined pump lasers with the same power per wavelength are more efficient. In terms of an FoM which depends on the achievable pump intensity and fiber loss, the conversion efficiency reaches 71% for FoM = 10, which is realistic with state-of-the-art pump sources. We considered a cladding/core area ratio of eight, for which the pump leakage is non-negligible. A smaller area ratio as well as core-pumping can reduce the pump leakage and thus improve the efficiency. The usable pump bandwidth reaches from 46 to 91 nm with the pump powers and wavelengths spacings considered. We expect that even higher usable pump bandwidths are possible with other parameters. For a given total pump bandwidth, the precise pump wavelengths have a relatively minor effect on the attainable conversion efficiency for the fixed and optimized wavelengths we have studied, but it does depend on the FoM. The general results apply also to single- and multimode core-pumping and to pumping with spectrally combined Yb-doped fiber lasers. Significantly, our results confirm that spectrally combined diode laser sources as currently being developed for materials processing can be used for high-power cladding-pumping of FRAs.

Acknowledgments

All data supporting this study are available from the University of Southampton at <https://doi.org/10.5258/SOTON/D0847>. This work was funded by AFOSR (FA9550-15-1-0041) and EPSRC (EP/P027644/1).

References

1. T. Yao et al., "High-power continuous-wave directly-diode-pumped fiber Raman lasers," *Appl. Sci.* **5**(4), 1323–1336 (2015).
2. J. Ji, C. A. Codemard, and J. Nilsson, "Brightness enhancement limits in pulsed cladding-pumped fiber Raman amplifiers," *Proc. SPIE* **7580**, 75801L (2010).
3. S. Zhu et al., "Multimode-pumped Raman amplification of a higher order mode in a large mode area fiber," *Opt. Express* **26**(18), 23295–23304 (2018).
4. J. Ji, "Cladding-pumped Raman fibre laser sources," Doctoral Thesis, University of Southampton, Optoelectronics Research Centre (2011).
5. E. A. Zlobina et al., "Generating high-quality beam in a multimode LD-pumped all-fiber Raman laser," *Opt. Express* **25**(11), 12581–12587 (2017).
6. L. Zhang et al., "Kilowatt Ytterbium-Raman fiber laser," *Opt. Express* **22**(15), 18483–18489 (2014).
7. H. Fritsche et al., "Highly modular high-brightness diode laser system design for a wide application range," *Proc. SPIE* **9348**, 93480A (2015).
8. J. Malchus et al., "A 40kW fiber-coupled diode laser for material processing and pumping applications," *Proc. SPIE* **9348**, 934803 (2015).
9. A. Sanchez-Rubio et al., "Wavelength beam combining for power and brightness scaling of laser systems," *Lincoln Lab. J.* **20**(2), 52–66 (2014).
10. S. Aparanji et al., "Simultaneous power combining and wavelength conversion of high power fiber lasers," in *Laser Congress 2017 (ASSL, LAC)*, Optical Society of America, p. ATu3A.4 (2017).
11. S. Hong, Y. Feng, and J. Nilsson, "Off-peak dual-wavelength multimode diode-laser-pumped fiber Raman laser," *IEEE Photonics Technol. Lett.* **30**(18), 1625–1628 (2018).
12. G. P. Agrawal, *Nonlinear Fiber Optics*, 4th ed., Elsevier, London (2006).
13. H. Kanamori et al., "Transmission characteristics and reliability of pure-silica-core single-mode fibers," *J. Light. Technol.* **4**(8), 1144–1150 (1986).
14. J. P. Kopolow, D. A. V. Kliner, and L. Goldberg, "Single-mode operation of a coiled multimode fiber amplifier," *Opt. Lett.* **25**(7), 442–444 (2000).
15. S. A. Babin et al., "Four-wave-mixing-induced turbulent spectral broadening in a long Raman fiber laser," *J. Opt. Soc. Am. B* **24**(8), 1729–1738 (2007).
16. W. Liu et al., "Modeling of the spectral evolution in a narrow-linewidth fiber amplifier," *Laser Phys. Lett.* **13**(3), 035105 (2016).
17. P. B. Hansen et al., "Rayleigh scattering limitations in distributed Raman pre-amplifiers," *IEEE Photonics Technol. Lett.* **10**(1), 159–161 (1998).
18. S. A. E. Lewis, S. V. Chernikov, and J. R. Taylor, "Characterization of double Rayleigh scatter noise in Raman amplifiers," *IEEE Photonics Technol. Lett.* **12**(5), 528–530 (2000).
19. B. Min, W. J. Lee, and N. Park, "Efficient formulation of Raman amplifier propagation equations with average power analysis," *IEEE Photonics Technol. Lett.* **12**(11), 1486–1488 (2002).
20. J. Ji et al., "Design, performance, and limitations of fibers for cladding-pumped Raman lasers," *Opt. Fiber Technol.* **16**(6), 428–441 (2010).
21. R. Chang et al., "Raman beam cleanup of a severely aberrated pump laser," *IEEE J. Quantum Electron.* **21**(5), 477–487 (1985).
22. J. Reintjes et al., "Beam cleanup with stimulated Raman scattering in the intensity-averaging regime," *J. Opt. Soc. Am. B* **3**(10), 1408–1427 (1986).
23. J. T. Murray, W. L. Austin, and R. C. Powell, "Intracavity Raman conversion and Raman beam cleanup," *Opt. Mater.* **11**(4), 353–371 (1999).
24. T. Russell, "Laser intensity scaling through stimulated scattering in optical fibers," Doctoral Thesis, Air Force Institute of Technology Wright-Patterson (2001).
25. T. H. Russell et al., "Stimulated Raman scattering in multi-mode fibers and its application to beam cleanup and combining," *J. Nonlinear Opt. Phys. Mater.* **11**(03), 303–316 (2002).

Soonki Hong is a PhD candidate at the Optoelectronic Research Centre, University of Southampton. He received his BS and MS degrees in physics from Seoul National University in 2010 and 2013, respectively. His current research interests include Raman fiber lasers, nonlinear optics, and high power fiber lasers.

Achar V. Harish received his doctorate from the Optoelectronics Research Centre (ORC), University of Southampton, United Kingdom, in 2017. He obtained his MSc degree from the Indian Institute of Technology Madras (IIT-M), Chennai, India. He has worked on optical fiber amplifiers and nonlinear fiber optics at ORC, and nondestructive testing with optical fiber sensors at IIT-M. His current research interests include suppression of stimulated Brillouin scattering in high power optical fiber amplifiers and nonlinear optics.

Johan Nilsson is a professor at the Optoelectronics Research Centre, University of Southampton, and head of the High Power Fibre Lasers research group. In 1994, he received a doctorate in Engineering Science from the Royal Institute of Technology (KTH), Sweden, and has since continued working on optical amplifiers and amplification in lightwave systems, optical communications, and guided-wave lasers, first at Samsung Electronics and later at ORC. He is a fellow of OSA and SPIE, advisor to ORC's SPIE student chapter, and a consultant and cofounder of SPI Lasers. He is a member of the advisory board of the *Journal of the Optical Society of Korea* and has served as a guest editor for several journals. He is currently a program chair for the Advanced Solid State Lasers conference and a member of the steering committee of the EuroPhoton conference.

Biographies of the other authors are not available.